Catalysis Today 148 (2009) 97–102

Contents lists available at ScienceDirect

Catalysis Today

journal homepage: www.elsevier.com/locate/cattod

# Effects of pre-treatment in air microwave plasma on the structure of CNTs and the activity of Ru/CNTs catalysts for ammonia decomposition

Jiuling Chen [a], Zhong Hua Zhu [a,*], Qing Ma [a], Li Li [a], Victor Rudolph [a], Gao Qing Lu [b]

[a] Division of Chemical Engineering, School of Engineering, The University of Queensland, St Lucia, Brisbane, QLD 4072, Australia
[b] ARC Centre of Excellence for Funtional Nanomaterials, The University of Queensland, St Lucia, Brisbane, QLD 4072, Australia

ARTICLE INFO

*Article history:*
Available online 13 March 2009

*Keywords:*
Ammonia decomposition
Carbon nanotubes
Ru catalyst
Hydrogen production

ABSTRACT

Carbon nanotubes (CNTs) were treated in air microwave plasma at three different microwave powers 80, 100 and 150 W. The effects of the treatment on the structure of CNTs and the dispersion of Ru particles supported on CNTs were evaluated using XRD, $N_2$ physisorption, FTIR, TPD, XPS, TEM and CO chemisorptions. The results show that the bulk structure and the texture of the CNTs were unchanged, but phenolic hydroxyls and carboxyls appeared on the surface. The total concentration of these groups increases with the microwave power to 100 W, then decreases. The phenolic hydroxyls and carboxyls on the CNTs interact with Ru ions during the preparation of Ru/CNTs resulting in highly dispersed Ru particles. The activity of Ru/CNTs for ammonia decomposition depends on the dispersion of Ru particles, but is negatively affected by any remaining oxygen-containing groups on the surface.



## 1. Introduction

The on-board generation of CO-free hydrogen is important for the commercialization of proton-exchange membrane fuel cells [1]. Even small CO concentrations of 10 ppm in the hydrogen seriously reduce the efficiency due to the adsorption of CO on the electrode catalysts within the cell [2,3]. Conventional processes for hydrogen production, such as steam reforming of methane or higher hydrocarbons, produce large amounts of CO and $CO_2$, requiring additional downstream treatment operations (such as water–gas shift, pressure-swing absorption and methanation) for their removal [3]. Ammonia presents an attractive hydrogen carrier for on-board vehicle generation without any CO contamination. Further, the small amount of unconverted ammonia can be reduced to less than 200 ppb level using an effective absorber [4–11].

Highly dispersed Ru particles supported on carbon nanotubes (Ru/CNTs) have been found to be much more active in ammonia decomposition than when supported on the other materials such as activated carbon, $Al_2O_3$ and MgO. The reason is because the electron transfer from CNTs to Ru particles is assisted by the high electronic conductivity of CNTs, inducing a decrease of the ionization potential of Ru and facilitating the rate of $N_2$ desorption, the control step in the process of ammonia decomposition [5–9,12–14].

It has been reported that the oxygen-containing functional groups, especially phenolic hydroxyls and carboxyls on the surface of CNTs are advantageous to producing a strong interaction between Ru and CNTs and obtaining the highly dispersed Ru particles, which can promote the activity of Ru/CNTs [5]. The surface of primitive CNTs is inert, presenting few anchor points for Ru particles [15]. Therefore, CNTs usually need to be pre-treated with strong oxidants, e.g. oxidizing gases such as ozone or nitric oxide or solutions (nitric acid, sodium hypochlorite, etc.), to introduce oxygen-containing functional groups such as phenolic hydroxyls and carboxyls which act as effective sites for particle binding [15–18]. However, these treatment methods are difficult to control and involve dangerous chemicals and difficult waste streams [17].

Microwave (MW) plasma with appropriate support gas offers a simple and efficient method for doping functional groups on the surface of many solid materials [19–21]. In this investigation, air MW plasma was employed to introduce oxygen-containing functional groups on the surface of CNTs. These arise from the reaction of carbon atoms of CNTs with highly active oxygen radicals produced within the MW [21]. The influence of the treatment on the structure and the texture of CNTs and the promoting effect on the activity of Ru/CNTs for ammonia decomposition were investigated.

## 2. Experimental

### 2.1. CNT treatment and loading of Ru

CNTs were obtained from Tsinghua University. These produced from methane decomposition on Fe-based catalyst at ca. 873–973 K

* Corresponding author. Tel.: +61 7 33653528; fax: +61 7 33654199.
*E-mail address:* z.zhu@uq.edu.au (Z.H. Zhu).

0920-5861/$ – see front matter © 2009 Elsevier B.V. All rights reserved.
doi:10.1016/j.cattod.2009.02.005

in a continuous commercial fluidized-bed reactor. The purity of the CNTs in the primitive samples is above 95%. The external diameter of CNTs is in the range of 10–30 nm with the majority around 20 nm. The inner diameters are typically about one-third of the corresponding external diameters. The carbon layers in a typical CNT are parallel to its axis.

The CNTs were first soaked in 4 M $HNO_3$ solution at room temperature for 24 h to remove any Fe particles carried over from the catalyst and then washed until neutrality. Following this step, the CNTs were dried in air at 393 K for 5 h and sieved into different size fractions. The particles in the range 63–500 μm were used for the doping experiments.

The plasma treatment of CNTs was carried out in a vertical quartz tube located inside the MW waveguide cavity. The MW magnetron provides 50–1000 W of power at a fixed frequency 2.45 GHz [22]. An infrared transducer was used to monitor the treatment temperature of the CNT samples. Approximately 1.0 g of CNTs was used for each experiment, which involved MW exposure for 5 min under air flow rate 120 ml $min^{-1}$ (STP) and pressure 60–90 Torr. Samples were produced at MW powers of 80, 100 and 150 W; the corresponding reflected powers were 2–3 W. We refer to these samples as follows: CNT-un (for CNT samples without treatment in plasma), CNT-80 (treatment at 80 W), CNT-100 (treatment at 100 W) and CNT-150 (treatment at 150 W).

The loading of Ru on the CNTs was done by dry impregnation method using an aqueous solution of $RuC1_3$. Analytical grade $RuCl_3{\cdot}3H_2O$ obtained from Sigma–Aldrich Inc. and without any further purification or drying, was used to prepare a 0.025 M aqueous solution of $RuC1_3$ whose pH value was about 5.5. After loading of $RuCl_3$, the samples were dried at room temperature in air for 24 h and then calcined in a quartz tube in atmosphere of $N_2$. This procedure used a heating rate of 2 K $min^{-1}$ from ambient to 773 K after which the sample was held at 773 K for 10 h. In all cases the Ru loading on the CNTs was 0.8 wt.%.

### 2.2. Characterization

The XRD measurements of the CNT samples before and after the treatment in air MW plasma were conducted with a Bruker D8 advance research X-ray diffractor (XRD) with Cu Kα radiation at a scanning rate of $2^\circ$ $min^{-1}$.

The pore structures of the samples were measured using nitrogen physisorption in an NOVA 1200 adsorption analyser (Quantachrome). Specific surface areas, Sg, of the samples were obtained from the BET equation. The pore size distributions of the samples were evaluated by the desorption branch of the isotherm using the BJH method.

The surface functional groups on CNT-un and CNT-100 were observed in a Nicolet NEXUS Fourier transform infrared spectroscopy (FTIR). CNT samples and KBr particles were first ground into fine particles smaller than 300 mesh, dried in air at 393 K for 5 h, cooled to ambient and kept in a drier, before being physically mixed with each other to uniformity and finally pressure formed into wafers. Since CNTs absorb infrared light strongly, the content of CNTs in the wafers was only 0.2–0.3 wt.%. During the investigation with FTIR, the wafers were located on the sample shelf which is exposed to air in the instrument available to us. The IR absorptions in the range of 3800–800 $cm^{-1}$ were recorded.

The desorption of CO and $CO_2$ from CNT-un, CNT-100 (without Ru impregnation) and from Ru/CNT-un and Ru/CNT-100 after reduction for 2 h in hydrogen at 773 K, was investigated in a temperature-programmed desorption (TPD) process. Helium was used as the carrier gas at a flow rate of 50 ml $min^{-1}$ (STP). The heating rate of the samples was 5 K $min^{-1}$. A Shimadzu GC-8A gas chromatograph equipped with a thermal conductivity detector (TCD) was employed to analyse the composition of the desorption gas.

The binding energies (BE) of O1s and the atomic ratios of O/C on the surface of the CNT samples were investigated with a PHI-560 ESCA system (PerkinElmer) X-ray photoelectron spectroscopy (XPS). C1s, 284.5 eV, was taken as a criteria. All spectra were acquired at a basic pressure $2 \times 10^{-7}$ Torr with Mg Kα excitation at 15 kV.

The morphology of the reduced Ru particles supported on CNTs was observed with a JEOL JEM 1010 transmission electron microscope (TEM).

CO chemisorption at room temperature was employed to measure the dispersion and the average size of Ru particles in a conventional pulse system. The samples were reduced in flowing hydrogen at 773 K for 2 h followed by flushing for 2 h in a helium stream of 50 ml $min^{-1}$ at 773 K and then cooled in flowing helium to ambient. CO pulses of 200 μl each were injected into the helium carrier gas and detected in the outlet gas by TCD. By comparing the amount of CO reaching the detector and the amount of CO injected, the quantity of CO adsorbed could be determined. Blank experiments on CNTs showed that there was no measurable uptake of CO on the support itself.

### 2.3. Ammonia decomposition

In the ammonia decomposition reaction, 100 mg catalyst samples were used for each experiment. A vertical quartz tube reactor with an inner diameter of 8 mm was used. The catalyst was first heated in pure hydrogen from ambient to 773 K at a heating rate of 5 K $min^{-1}$ and then held for 2 h to reduce the catalyst fully. Finally the temperature of the catalyst was adjusted to the required temperature and the feed was switched from hydrogen to argon to flush the system for 30 min and then switched to ammonia for the decomposition reaction. Pure ammonia with a flow rate of 70 ml $min^{-1}$ (STP) was used as reactant. All the reactions were performed at atmospheric pressure. The same gas chromatograph as above equipped with a TCD was used to analyse the composition of the product gas. Argon was used as the carrier gas.

## 3. Results and discussion

### 3.1. Effects of air plasma treatment on the texture and structure of CNTs

During the treatment of CNTs in air MW plasma, the colour of the plasma ball was purple, becoming brighter as the MW power was increased. The temperatures of the treated CNTs were 853, 883 and 933 K for MW output powers of 80, 100 and 150 W, respectively. Since some CNT samples were lost down stream into the vacuum pump during the treatment process, the mass change due to oxidization could not be obtained.

The XRD profiles of the four different CNT samples are shown in Fig. 1. The structures of all the CNTs before and after treatment in air MW plasma at 80–150 W are similar to that of graphite crystal, which means the treatment does not change the bulk structure of the CNTs.

The pore size distribution curves of CNT-un, CNT-80, CNT-100 and CNT-150 obtained from $N_2$ physisorption are shown in Fig. 2. There is no clear change except for a slight volume increase of the pores between 12.5 and 15 nm in CNT-80 and between 2.5 and 3.7 nm in CNT-100. The corresponding surface areas (Sg) of CNT-un, CNT-80, CNT-100 and CNT-150 are 160, 155, 167 and 141 $m^2$ $g^{-1}$, respectively. The pore size distributions and the values of Sg for all the samples are essentially equivalent considering the resolution of the adsorption instrument.

These results with XRD and $N_2$ physisorption indicate that the MW treatment did not alter the bulk structure and the texture, which is advantageous to the use of CNTs as a support for Ru catalyst.

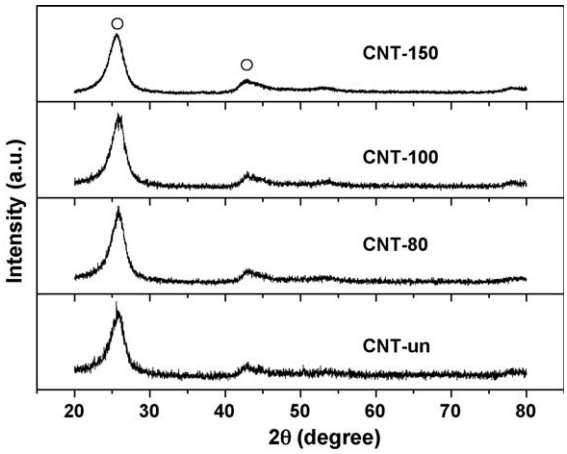


**Fig. 1.** XRD profiles of the CNT samples before and after treatment in air MW plasma at different MW powers; Cu Kα; O, graphite.

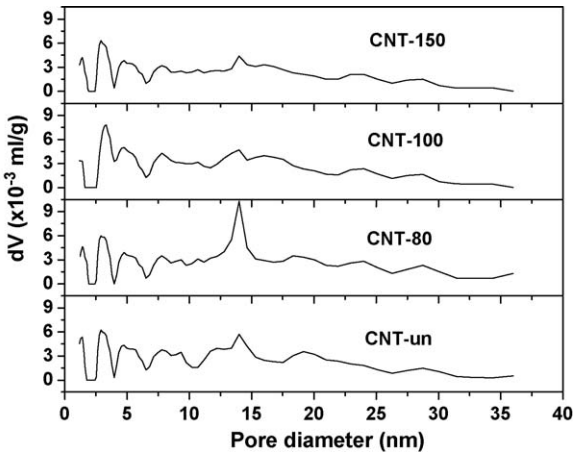


**Fig. 2.** Pore size distributions of the CNT samples measured before and after treatment in air MW plasma at different MW powers.

### 3.2. Effects of plasma treatment on the surface functional groups of CNTs

Fig. 3 shows the IR absorption spectra of CNT-un and CNT-100 in the range of 3800–800 $cm^{-1}$. All band assignments are summarised in Table 1.

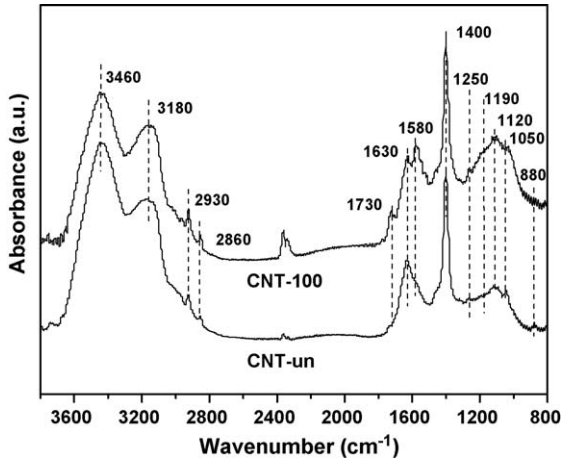


**Fig. 3.** IR absorption spectra of the untreated CNT sample (CNT-un) and treated in air MW plasma at 100 W of MW power (CNT-100).

**Table 1**
Assignments of the absorption peaks in IR spectra of CNT-un and CNT-100.

| $\sigma$ ($cm^{-1}$) | Assignments | References |
|---|---|---|
| 880 | Isolated aromatic C–H out-of-plane bending | [16] |
| 1050–1120 | C–O stretching in ethers | [23,24] |
| 1190 | C–C stretching | [16] |
| 1250 | C–O stretching in phenols | [23,24] |
| 1400 | H–O bending in water, carboxyls and phenols | [16,25,26] |
| 1580 | Aromatic ring stretching | [16,18,23] |
| 1630 | Adsorbed water | [16,25] |
| 1730 | C═O stretching in carbonyls and carboxyls | [16,18,23,25] |
| 2860, 2930 | $CH_2/CH_3$ stretching | [16,23] |
| 3180 | H–O stretching in carboxyls and phenols | [23,24] |
| 3460 | H–O stretching in water | [27,28] |

For the spectrum of CNT-un, the peak at 880 $cm^{-1}$ is ascribed to the isolated aromatic C–H out-of-plane bending mode [16]; the peaks at 1050 and 1120 $cm^{-1}$ are due to the stretching vibrations of C–O in ethers [23,24]; the peak at 1250 $cm^{-1}$ comes from the stretching vibrations of C–O in phenols [23,24]; the absorptions at 1630 $cm^{-1}$ are due to water adsorbed mainly on the KBr and CNTs, possibly during the preparation and the observation [16,25]; since no peaks appear at 1730 $cm^{-1}$ (assigned to the stretching vibration of C═O) [16,18,23,25], the peak at 1400 $cm^{-1}$ may be in associated with H–O bending vibrations in water and phenols [16,25,26] and the peak at 3180 $cm^{-1}$ may be attributed to H–O stretching vibration in phenols [23,24]; the peaks of 2860 and 2930 $cm^{-1}$ are in the range of $CH_3/CH_2$ stretching vibration [16,23]. The absorptions at 3460 $cm^{-1}$ is due to the H–O stretching vibration of the adsorbed water on the KBr and CNTs [27,28]. The absorptions at 1400, 1630 and 3460 $cm^{-1}$ are also present in the KBr backgrounds. In this interpretation, besides C–C and C–H, there are oxygen-containing surface groups on CNT-un, mainly ethers together with some phenols. These groups most likely arise in the pre-treatment in 4 M $HNO_3$ solution at room temperature. Also, oxygen in air may be chemisorbed at low temperatures on unsaturated carbon atoms at any defects or dislocations that occur on the surface of the CNTs. These may react further to generate some of the oxygen-containing surface groups [15].

Compared with IR spectrum of CNT-un, two additional bands are apparent on CNT-100: one is at 1580 $cm^{-1}$ originating from an aromatic ring vibration [16,18,23]; and the other is at 1730 $cm^{-1}$ which can be assigned to the C═O stretching vibration in carboxyls or carbonyls [16,18,23,25]. The peak at 1580 $cm^{-1}$ indicates aromatic skeleton rings sticking out of the surface of CNTs after the oxidation of the surface in air MW plasma. The formation of C═O shows oxidization to generate carbonyls or carboxyls in the surface of CNT-100. Additionally, the absorptions at 1190 $cm^{-1}$ which correspond to C–C stretching vibrations are enhanced and the peak at 880 $cm^{-1}$ becomes obscure, which implies C–H bonds were oxidized and more carbon defects appeared on the surface of CNTs [16]. The increased intensity of the peak at 1250 $cm^{-1}$ indicates more phenols were formed [23,24]. The increased intensity of the peak at 3180 $cm^{-1}$ shows comparatively more phenols and carboxyls in the surface of CNT-100. Since the surface functional groups are very complex and their vibration ranges are adjacent to one another, it is difficult to make quantitative assignments. Nevertheless, the above analysis shows that more carboxyls and phenols were produced after MW treatment.

TPD spectra of CNT-un and CNT-100 are shown in Fig. 4A and B. In all cases, an increase of the amount of the surface oxygen-containing groups is evidenced by the bigger peak areas of CO and $CO_2$. According to the literature [29], the formation temperatures of CO and $CO_2$ correspond to the different kinds of the surface oxygen-containing groups. Phenols may decompose to CO at low temperatures around 873 K, compared with ethers, carbonyls and

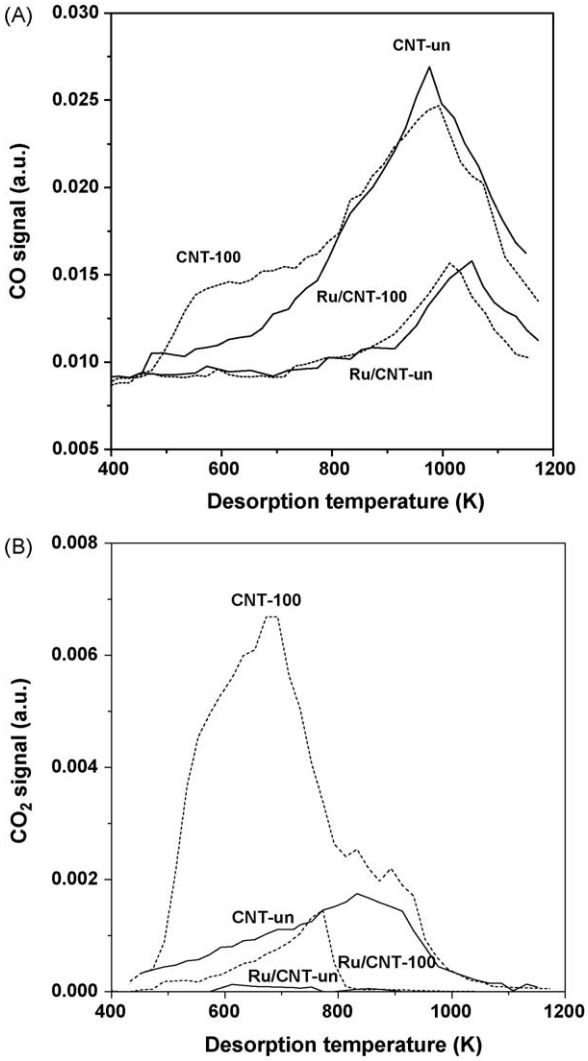


**Fig. 4.** TPD spectra for the untreated CNT sample (CNT-un), the treated sample in air MW plasma at 100 W of MW power (CNT-100) and the two reduced Ru catalysts with hydrogen at 773 K, Ru/CNT-un and Ru/CNT-100; (A) CO evolution; (B) $CO_2$ evolution.

quinones at high temperatures, 873–1253 K. The decomposition of carboxyls and lactones to $CO_2$ occurs at 373–673 and 463–900 K, respectively. Anhydrides decompose to CO and $CO_2$ at about 623–900 K. In Fig. 4A, CNT-100 gives much more CO than CNT-un in the range 500–800 K, while the amounts of CO formed on them are comparable above 800 K. In Fig. 4B, the $CO_2$ signal of CNT-100 is much pronounced than that of CNT-un: for CNT-100, there are big peaks at 480–800 K and some shoulder peaks from 800 to 1100 K; for CNT-un, the main peaks appear around 850 K. After considering these results together with the above FTIR results, we ascribe the shoulder CO peak of CNT-100 at 480–800 K to phenols, and the big CO peaks of both CNT-un and CNT-100 above 800 K to the decomposition of ethers [29]. The $CO_2$ peaks of CNT-100 at 400–800 K are assigned to carboxyls. The shoulder peaks of CNT-100 at 800–1100 K and the peaks of CNT-un around 850 K may be due to lactones and anhydride. The reason that no C═O on CNT-un could be seen with FTIR may be because the amount is too low. TPD results further show that after the treatment in plasma at 100 W, the concentration of ethers on the surface of the CNTs was not appreciably changed, the increase of lactones and anhydrides was slight, but there was a pronounced increase in phenols and carboxyls. This is consistent with FTIR results.

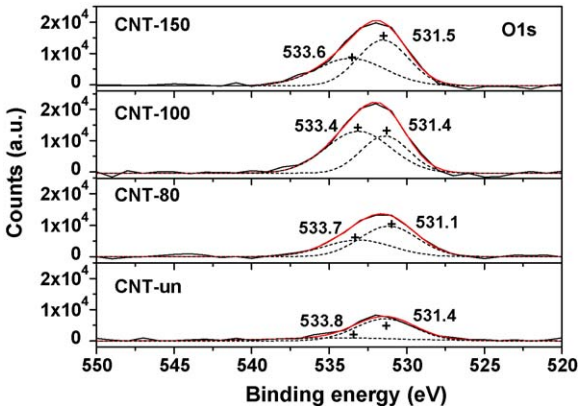


**Fig. 5.** Binding energies of O1s on the CNT samples before and after treatment in air MW plasma at different MW powers.

Fig. 5 shows the O1s core level spectra of XPS of CNT-un, CNT-80, CNT-100 and CNT-150. The O1s spectra of the four samples are subdivided into two Gaussian sub-peaks. The details of the fitting results of the peaks, such as BE, full widths at half maximum (FWHM) and areas of the peaks are given in Table 2. Peak I at 531.1–531.5 eV represents oxygen in C–O and C═O bonds, and peak II at 533.4–533.8 eV is attributed to oxygen in H–O bonds [19,30,31]. However, no peaks are found at 535.9 eV which corresponds to oxygen in the chemisorbed water which may be observed on both CNT-un and CNT-100 with FTIR [29]. We consider that these water molecules were most likely desorbed from the surface of CNTs as a result of being bombarded by high energy $Ar^+$ ions in vacuum during XPS measurements.

The changes in BE of O1s here can be considered insignificant based on the energy resolution of the XPS instrument. After considering the TPD and FTIR results, majority of the oxygen-containing surface groups are ethers and the concentration of phenolic hydroxyls and carboxyls is very low on CNT-un. From CNT-un to CNT-80 to CNT-100, the concentrations of both C–O/C═O and of H–O increase, which means more phenolic hydroxyls and carboxyls were produced from the air plasma treatment. From CNT-100 to CNT-150, the concentration of C–O/C═O goes up, while that of H–O decreases. The measured atomic ratios of O/C in CNT-un, CNT-80, CNT-100 and CNT-150 are 0.03:1, 0.05:1, 0.10:1 and 0.09:1. A MW power increase from 100 to 150 W, should make the oxygen radicals in the air MW plasma more active and consequently lead to the further oxidization of phenolic hydroxyls to carbonyls. The corresponding increase of the treatment temperature of CNTs from 883 to 933 K as the power is increased may be expected to lead to esterification and dehydration among phenolic hydroxyls and carboxyls. All these reactions lead to a decrease the concentration of phenolic hydroxyls and carboxyls in the surface of the CNTs. The competing factors result in a maximum in the concentration of phenols and carboxyls on the surface of CNTs, which occurs around 100 W of MW power in our apparatus.

**Table 2**
Results of the deconvolution of XPS spectra of the O1s region using a multiple Gaussian function.

| CNT samples | Peak I (C–O/C═O) | | | Peak II (O–H) | | |
|---|---|---|---|---|---|---|
| | BE (eV) | FWHM (eV) | Area | BE (eV) | FWHM (eV) | Area |
| CNT-un | 531.4 | 4.8 | 34,000 | 533.8 | 10.2 | 11,000 |
| CNT-80 | 531.1 | 4.4 | 46,000 | 533.7 | 5.2 | 30,000 |
| CNT-100 | 531.4 | 3.5 | 47,000 | 533.4 | 4.9 | 70,000 |
| CNT-150 | 531.5 | 3.8 | 60,000 | 533.6 | 4.9 | 49,000 |

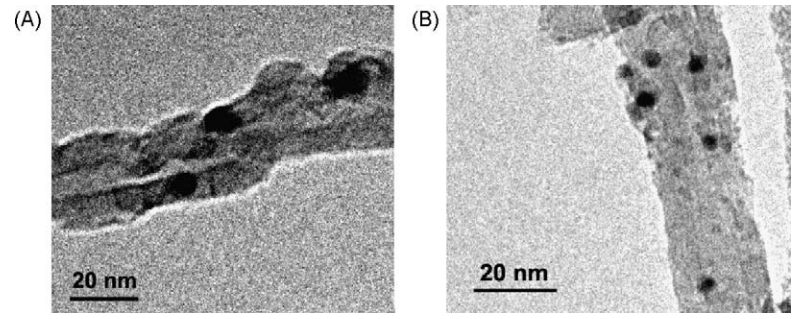


**Fig. 6.** Ru particles supported on the untreated CNT sample (CNT-un) and the treated sample in air MW plasma at 100 W of MW power (CNT-100); (A) on CNT-un; (B) on CNT-100.

To investigate the remaining oxygen-containing surface groups on Ru/CNTs catalysts, the evolution spectra of CO and $CO_2$ were observed in TPD processes of Ru/CNT-un and Ru/CNT-100 following reduction in hydrogen at 773 K, as depicted in Fig. 4A and B. The concentration of oxygen-containing groups decreases sharply after reduction. The remaining phenols and ethers on Ru/CNT-100 were similar to those on Ru/CNT-un. Anhydrides and lactones on Ru/CNT-un decomposed nearly completely, while some carboxyls, lactones and anhydrides could still be observed on Ru/CNT-100.

### 3.3. Effects of air plasma treatment on the catalyst dispersion

Two typical TEM microphotos are shown in Fig. 6A and B. Based on TEM the majority of the Ru particle sizes on CNT-un and CNT-100 after reduction at 773 K were around 15 and 5 nm, respectively. It should be specified that we cannot clearly identify whether the Ru particles are located inside or outside the tubes because the TEM image is of two dimensions. No residual iron catalyst from the primitive CNT samples were found with TEM, demonstrating that soaking in 4 M $HNO_3$ solution was effective for iron removal.

CO chemisorption was used to measure the dispersion of Ru particle, $D_{Ru}$, and the average size of Ru particle, $d_{Ru}$. The surface area of Ru metal particles was calculated assuming a Ru surface density of $1.63 \times 10^{19}$ atoms $m^{-2}$, a stoichiometry CO:Ru = 1:1, and a hemisphere model of a Ru particle contacting with the CNT support surface. The average Ru particle size, $d_{Ru}$ was determined by the expression $d_{Ru} = 6V/S$, where $V$ and $S$ are the metal volume and the surface area of Ru, respectively [32,33]. The measurement results of $D_{Ru}$ and $d_{Ru}$ on Ru/CNT-un, Ru/CNT-80, Ru/CNT-100 and Ru/CNT-150 are given in Table 3.

The absolute sizes of Ru particle obtained with CO chemisorption are smaller than the corresponding values by TEM observation, which reflects the different measurement methods. However, both the results indicate that the dispersion of Ru particles is significantly improved after the treatment of the CNTs in air MW plasma.

Phenolic hydroxyls and carboxyls have a major effect on the dispersion of metal particles on carbon materials during impregnation [5,15]. First, these groups decrease the hydrophobicity of the carbon surface thus making it more accessible to the aqueous metal precursor solution. Most dilute aqueous $Ru^{3+}$ from $RuCl_3$ exist as $[Ru(H_2O)_5Cl]^{2+}$, $[Ru(H_2O)_5OH]^{2+}$ and $[Ru(H_2O)_6]^{3+}$ [34] which interact with the acidic phenolic hydroxyls and carboxyls. The chemical interaction between $Ru^{3+}$ groups and the surface $–O^-$ and $–COO^-$ serves to hinder agglomeration and surface diffusion of $Ru^{3+}$ ions, and minimizes the sintering propensity of the formed Ru particles across the CNT surface in the calcination and reduction process [15]. The peak concentration of phenolic hydroxyls and carboxyls that occurs around at 100 W of MW power, results in the most Ru anchor points for Ru particles and maximizes the interaction between CNT surface and the Ru particles, for the conditions applied in this investigation.

**Table 3**
The dispersion and the average particle size of Ru supported on CNTs measured by the chemisorption of CO pulse.

| Samples | Weight of samples (mg) | Volume of adsorbed CO (μl) | $D_{Ru}$ (%) | $d_{Ru}$ (nm) |
|---|---|---|---|---|
| Ru/CNT-un | 500 | 138 | 16 | 8.6 |
| Ru/CNT-80 | 480 | 142 | 17 | 8.1 |
| Ru/CNT-100 | 432 | 254 | 33 | 4.1 |
| Ru/CNT-150 | 453 | 240 | 30 | 4.5 |

### 3.4. Activity of Ru/CNTs in ammonia decomposition

Fig. 7A and B shows the rate of ammonia conversion based on the weight of Ru employed and the turnover frequencies (TOF) of ammonia conversion based on the number of Ru atoms available on the surface of the Ru particles at 773, 823 and 873 K, respectively. Ru is an expensive metal, and from a technological perspective a high rate of ammonia conversion, related to its mass, is a key criterion of the catalyst's usefulness [35]. However, a scientific understanding is also of importance so the surface activity, expressed in TOF of ammonia, is also provided.

From Fig. 7A, the rate of ammonia conversion increases from Ru/CNT-un to Ru/CNT-80 to Ru/CNT-100. However, the rate of ammonia conversion is lower on Ru/CNT-150 than that on Ru/CNT-100. From Fig. 7B, Ru/CNT-un and Ru/CNT-80 have a much higher TOF than Ru/CNT-100 or Ru/CNT-150.

Having established that the treatments do not change the bulk structure and the texture of the CNTs and since all the Ru/CNTs catalyst samples were prepared using the same experimental procedure, their differences in activity with respect to ammonia decomposition are attributed to the interaction of Ru particles with phenolic hydroxyls and carboxyls located on the surface of the CNTs [15].

It has been reported that the process of $N_2$ desorption on the surface of Ru is a structure sensitive reaction and related to ensembles of Ru atoms ($B_5$-type active sites) on the surface of Ru particles [35,36]. The maximum probability for $B_5$-type active sites occurs for Ru particles of 1.8–2.5 nm. For particles larger than that, the probability monotonically decreases [36]. Therefore, increasing the dispersion of Ru particles should be advantageous for promoting the activity of Ru/CNTs in ammonia decomposition [5]. On the other hand, the remaining surface oxygen-containing groups located on Ru/CNTs have been found to decrease the surface activity of Ru [8,9,13,14] as a result of electron withdrawal, which can be shown by the decrease of the values of TOF of ammonia. Since the electron-drawing interaction is only local, this negative effect should be weaker for larger Ru particles [35]. Therefore, the activity of Ru/CNTs in ammonia decomposition is dependent on

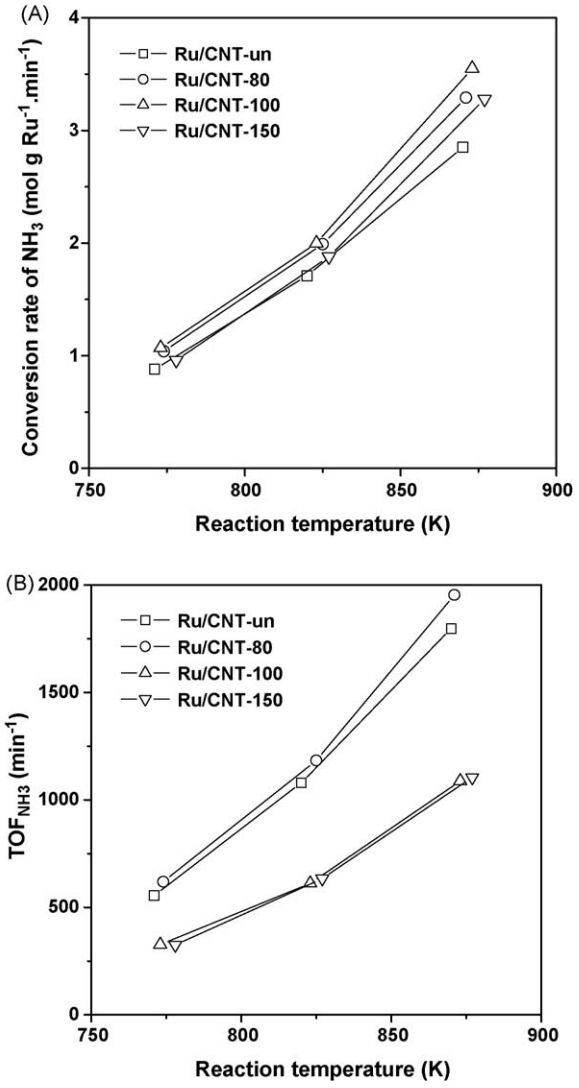


**Fig. 7.** Rate of ammonia conversion and turnover frequency of $NH_3$ in ammonia decomposition on Ru catalysts supported on untreated CNT sample and the treated samples in air MW plasma at different MW powers; (A) rate of $NH_3$ conversion; (B) turnover frequency of $NH_3$.

the positive effects from dispersion of Ru particles and the negative effect of the remaining oxygen-containing groups on the surface of CNTs.

Based on this analysis, Ru/CNT-un to Ru/CNT-80 should have a smaller number of $B_5$-type active sites per gram of Ru than Ru/CNT-150 to Ru/CNT-100 as the former two have a larger catalyst particle size as shown in Table 3. Fig. 7B shows that the Ru/CNT-un to Ru/CNT-80 have a much higher TOF than Ru/CNT-150 to Ru/CNT-100. Therefore, the negative effect of the remaining oxygen-containing groups on Ru/CNT-un or Ru/CNT-80 is much weaker than that on Ru/CNT-100 or Ru/CNT-150. This balance results in an optimum (for ammonia decomposition) at about Ru/CNT-100.

## 4. Conclusions

The bulk structure and the texture of CNTs remain unchanged after the treatment of CNTs in air MW plasma at 80–150 W of MW power in this investigation. However, the acidic groups, phenolic hydroxyls and carboxyls appear on the surface of CNTs during the treatment process. The total concentration of them increases with the treatment MW power till 100 W. When the power is 150 W, owing to the increase of the treatment temperature and the activity of the oxygen radicals, the further reaction processes may decrease the total concentration. Phenolic hydroxyls and carboxyls play an important role to decrease the size of Ru particles supported on CNTs and increase their dispersion. The activity of Ru/CNTs in ammonia decomposition depends on the balance between the size of the Ru particles and the negative effect of the remaining oxygen-containing groups on the surface of Ru/CNTs. The optimal power of air MW plasma is 100 W for the treatment of CNT, which results in the highest catalyst activity for Ru/CNTs-100.

## Acknowledgment

This project is supported by the Australian Research Council.

## References

[1] R.A. Lemons, J. Power Sources 29 (1990) 251.
[2] C.S. Song, Catal. Today 77 (2002) 17.
[3] T.V. Choudhary, C. Sivadinarayana, D.W. Goodman, Chem. Eng. J. 93 (2003) 69.
[4] A.S. Chellappa, C.M. Fischer, W.J. Thomson, Appl. Catal. A 227 (2002) 231.
[5] S.F. Yin, B.Q. Xu, C.F. Ng, C.T. Au, Appl. Catal. B 48 (2004) 237.
[6] L. Li, Z.H. Zhu, Z.F. Yan, G.Q. Lu, L. Rintoul, Appl. Catal. A 320 (2007) 166.
[7] L. Li, Z.H. Zhu, G.Q. Lu, Z.F. Yan, S.Z. Qiao, Carbon 45 (2007) 11.
[8] S.F. Yin, B.Q. Xu, W.X. Zhu, C.F. Ng, X.P. Zhou, C.T. Au, Catal. Today 93–95 (2004) 27.
[9] S.F. Yin, B.Q. Xu, S.J. Wang, C.F. Ng, C.T. Au, Catal. Lett. 96 (2004) 113.
[10] T.V. Choudhary, C. Sivadinarayana, D.W. Goodman, Catal. Lett. 72 (2001) 197.
[11] T.V. Choudhary, D.W. Goodman, Catal. Today 77 (2002) 65.
[12] H.S. Zeng, K. Inazu, K. Aika, J. Catal. 211 (2002) 33.
[13] K. Aika, K. Shimazaki, Y. Hattori, A. Ohya, S. Ohshima, K. Shirota, A. Ozaki, J. Catal. 92 (1985) 296.
[14] K. Aika, A. Ohya, A. Ozaki, Y. Inoue, I. Yasumori, J. Catal. 92 (1985) 305.
[15] F. Rodriguez-Reinoso, Carbon 36 (1998) 159.
[16] T.G. Ros, A.J. van Dillen, J.W. Geus, D.C. Koningsberger, Chem. Eur. J. 8 (2002) 1151.
[17] P. Serp, M. Corrias, P. Kalck, Appl. Catal. A 253 (2003) 337.
[18] Y.Q. Liu, L. Gao, Carbon 43 (2005) 47.
[19] Y.S. Kim, J.H. Cho, S.G. Ansari, H.I. Kim, M.A. Dar, H.K. Seo, G.S. Kim, D.S. Lee, G. Khang, H.S. Shin, Synth. Met. 156 (2006) 938.
[20] Y. Sakamoto, M. Takaya, Surf. Coat. Technol. 169–170 (2003) 321.
[21] Q.H. Jin, S.S. Dai, K.M. Huang (Eds.), Weibo Huaxue (Microwave Chemistry), Science Press, Beijing, 1999.
[22] H.W. Chen, V. Rudolph, Diamond Relat. Mater. 12 (2003) 1633.
[23] P.E. Fanning, M.A. Vannice, Carbon 31 (1993) 721.
[24] E. Papirer, E. Guyon, N. Perol, Carbon 16 (1978) 133.
[25] M.S.P. Shaffer, X. Fan, A.H. Windle, Carbon 36 (1998) 1603.
[26] C. Moreno-Castilla, M.V. Lopez-Ramon, F. Carrasco-Marin, Carbon 38 (2000) 1995.
[27] H. Kandori, Y. Shichida, J. Am. Chem. Soc. 122 (2000) 11745.
[28] W. Neagle, C.H. Rochester, J. Chem. Soc. Faraday Trans. 86 (1990) 181.
[29] J.L. Figueiredo, M.F.R. Pereira, M.M.A. Freitas, J.J.M. Orfao, Carbon 37 (1999) 1379.
[30] J. Cui, W.P. Wang, Y.Z. You, C.H. Liu, P.H. Wang, Polymer 45 (2004) 8717.
[31] T.I.T. Okpalugo, P. Papakonstantinou, H. Murphy, J. Mclaughlin, N.M.D. Brown, Carbon 43 (2005) 153.
[32] J.R. Anderson, Surface of Metallic Catalysts, Academic Press, New York, 1975.
[33] G. Nerl, R. Pietropaolo, S. Galvagno, C. Milone, J. Schwank, J. Chem. Soc. Faraday Trans. 90 (1994) 2803.
[34] S.K. Tyrlik, K. Kurzak, Transit. Met. Chem. 20 (1995) 330.
[35] W. Raróg-Pilecka, E. Miśkiewicz, D. Szmigiel, Z. Kowalczyk, J. Catal. 231 (2005) 11.
[36] C.J.H. Jacobsen, S. Dahl, P.L. Hansen, E. Törnqvist, L. Jensen, H. Topsøe, D.V. Prip, P.B. Møenshaug, I. Chorkendorff, J. Mol. Catal. A 163 (2000) 19.